Molecular Therapy
Original Article

LIGHT/TNFSF14 promotes CAR-T cell trafficking and cytotoxicity through reversing immunosuppressive tumor microenvironment

Na Zhang,[1,2,6] Xiaohong Liu,[1,6] Juliang Qin,[1,6] Yue Sun,[1] Hao Xiong,[1] Boxu Lin,[1] Kexin Liu,[2] Binghe Tan,[2] Chenglin Zhang,[3] Chenshen Huang,[4] Shancheng Ren,[5,6] Mingyao Liu,[1] and Bing Du[1]

[1]Shanghai Frontiers Science Center of Genome Editing and Cell Therapy, Shanghai Key Laboratory of Regulatory Biology and School of Life Sciences, East China Normal University, Shanghai 200241, China; [2]BRL Medicine, Inc, Shanghai 201109, China; [3]Department of Orthopedics, Shanghai Changzheng Hospital, Shanghai 200003, China; [4]Department of Gastrointestinal Surgery, Fujian Provincial Hospital, Shengli Clinical Medical College of Fujian Medical University, Fuzhou 350001, China; [5]Department of Urology, Shanghai Changzheng Hospital, Shanghai 200003, China

Tertiary lymphoid structures (TLSs) in tumor tissues facilitate immune cell trafficking and cytotoxicity, which benefits survival and favorable responses in immune therapy. Here, we observed a high correlation of tumor necrosis factor superfamily member 14 (LIGHT) expression with TLS signature genes, which are all markers for immune cell accumulation and better prognosis, through retrieving RNA sequencing (RNA-seq) data from patients with cancer, suggesting the potential of LIGHT in reconstituting a high immune-infiltrated tumor microenvironment. Accordingly, LIGHT co-expressed chimeric antigen receptor T (LIGHT CAR-T) cells not only showed enhanced cytotoxicity and cytokine production but also improved CCL19 and CCL21 expression by surrounding cells. And the supernatant of LIGHT CAR-T cells promoted T cell migration in a paracrine manner. Furthermore, LIGHT CAR-T cells showed superior anti-tumor efficacy and improved infiltration in comparison with conventional CAR-T cells in immunodeficient NSG mice. Accordingly, murine LIGHT-OT-1 T cells normalized tumor blood vessels and enforced intratumoral lymphoid structures in C57BL/6 syngeneic tumor mouse models, implying the potential of LIGHT CAR-T in clinical application. Taken together, our data revealed a straightforward strategy to optimize trafficking and cytotoxicity of CAR-T cells by redirecting TLSs through LIGHT expression, which has great potential to expand and optimize the application of CAR-T therapy in solid tumors.

INTRODUCTION

Although chimeric antigen receptor (CAR) T cells have shown great therapeutic success in hematological cancers,[1] limited responses in solid tumors restricted the further application of CAR-T therapy to fulfill the huge unmet clinical needs.[2] A major obstacle to develop long-term effective CAR-T therapy is poor T cell infiltration to the suppressive tumor microenvironment, especially in typical "cold" prostate cancer (prostate adenocarcinoma [PRAD]). Although engineering T cells with chemokine receptors and adhesion molecules theoretically improves the infiltration of adoptively transferred T cells to tumors,[3,4] the complicated and distinct chemokines set in different tumors hinders the improvement of anti-tumor immune responses. Instead, CAR-T cells with extrinsic chemokine expression not only promote the infiltration of T cells but also increase the recruitment of supporting cells that facilitate the efficacy of cancer immunotherapy. For example, CCL19/CCL21 contributed to maintenance of the lymphoid structure via recruitment of $CCR7^+$ immune cells, including naive and central memory T cells, as well as activating dendritic cells (DCs).[5] Accordingly, engineered CAR-T cells with interleukin-7 (IL-7) and CCL19 (7×19 CAR),[6] or IL-7 and CCL21 (7×21 CAR),[7] improve the infiltration, accumulation, and survival of CAR-T cells in various solid tumors, whereas extrinsic chemokine expression is not sufficient to reverse the suppressive tumor microenvironment, and the benefits to patients is still far from satisfactory.

More and more evidence has demonstrated that reconstitution of tertiary lymphoid structures (TLSs) in the tumor microenvironment benefits the clinical outcome of cancer immunotherapy. Thus, exploring the key components involved in TLS formation is important for developing new strategies for immunotherapy to solid tumors. LIGHT, also known as tumor necrosis factor superfamily member 14 (TNFSF14/CD258), is mainly expressed on activated T cells and natural killer (NK) cells, as well as immature DCs, and facilitates

Received 4 October 2022; accepted 28 June 2023;
https://doi.org/10.1016/j.ymthe.2023.06.015.

[6]These authors contributed equally

Correspondence: Shancheng Ren, PhD, Department of Urology, Shanghai Changzheng Hospital, Shanghai 200003, China.
E-mail: renshancheng@gmail.com
Correspondence: Mingyao Liu, PhD, Shanghai Frontiers Science Center of Genome Editing and Cell Therapy, Shanghai Key Laboratory of Regulatory Biology and School of Life Sciences, East China Normal University, Shanghai 200241, China.
E-mail: myliu@bio.ecnu.edu.cn
Correspondence: Bing Du, PhD, Shanghai Frontiers Science Center of Genome Editing and Cell Therapy, Shanghai Key Laboratory of Regulatory Biology and School of Life Sciences, East China Normal University, Shanghai 200241, China..
E-mail: bdu@bio.ecnu.edu.cn

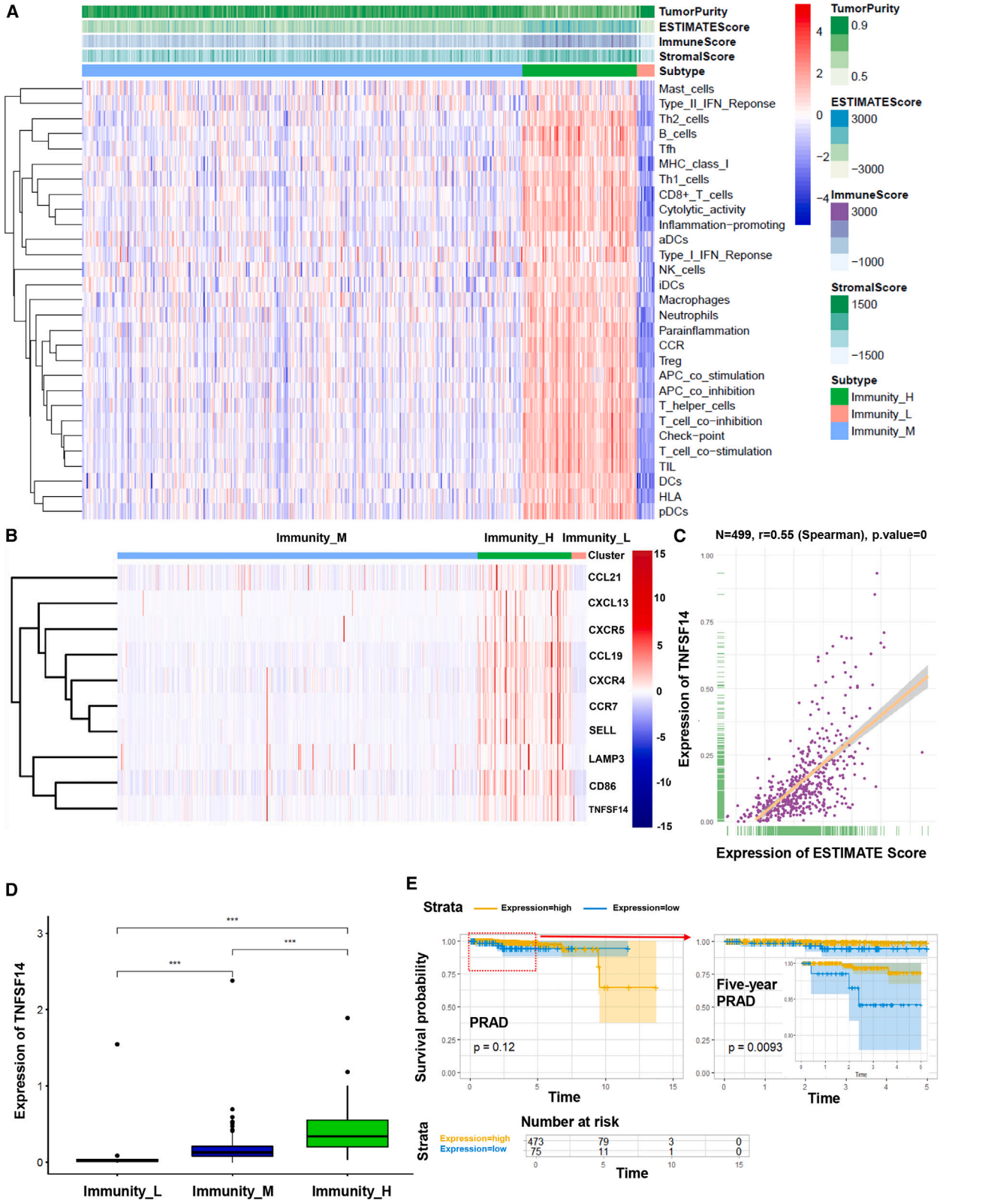

(legend on next page)

TLS formation in tumor tissues through inducing tumor vasculature normalization and high endothelial venule formation.[8,9] LIGHT functions in both a soluble and cell surface-bound manner to interact with two primary functional receptors: herpes virus entry mediator (HVEM) and lymphotoxin-β receptor (LTβR). The LIGHT-HVEM interaction is responsible for enhanced T cell activation, proliferation, survival, and Th1 cytokine production,[10–12] whereas LIGHT-LTβR signaling increases the susceptibility of cancer cells to immune responses, reconstituting chaotic tumor vasculature and supporting effector cell infiltration into tumors through providing crucial signals for the TLS formation.[13–15] However, the application of LIGHT in reconstitution of the anti-tumor immune microenvironment for adoptive immune cell therapy has been little explored.

In this study, we co-expressed soluble LIGHT with a vascular targeting peptide (VTP) in CAR-T cells to overcome the dilemmas of immunotherapy to solid tumors. The secreted LIGHT not only activated HVEM to increase the cytotoxicity of CAR-T cells but also reshaped the immunosuppressive tumor microenvironment through LTβR on the surrounding cells. Accordingly, CCL19 and CCL21, which are markers for TLSs, were enhanced obviously in LIGHT co-expressing CAR-T cells both *in vitro* and *in vivo*. Meanwhile, the infiltration and cytotoxicity of CAR-T cells to the cancer cells were improved significantly in both prostate cancer and a melanoma mouse model, suggesting the great potential of LIGHT in facilitating CAR-T therapy to solid tumors.

RESULTS

LIGHT is a potential enhancer for cancer immunotherapy

To investigate the correlation of tumor-associated TLSs with favorable prognosis in various type of human cancers, we retrieved RNA sequencing (RNA-seq) data for pan-cancer from The Cancer Genome Atlas (TCGA) database, and the TLS signature gene set was used to generate a Kaplan-Meier plot to confirm the importance of TLSs in cancer.[16] Then, we classified PRAD into three distinct subtypes by immunogenomic profiling: immunity high (Immunity_H), immunity medium (immunity_M), and immunity low (Immunity_L) on the basis of single-sample gene set enrichment analysis (ssGSEA) scores of the 29 gene sets as previous described to explore the potential regulators for high TLS subtypes.[17] The clustering results demonstrated that Immunity_H, which represents higher tumor immune infiltration, only accounts for a small part in all patients (Figure 1A). What's more, the Immunity_H subtype has high expression of identified TLS signature genes including CCL19, CCL21, CXCL13, CCR7, CXCR4, CXCR5, CD86, SELL, and LAMP3, as well as LIGHT/TNFSF14 (Figure 1B). In addition, LIGHT is positively correlated with the immune ESTIMATE score (Figure 1C), which provides crucial signals for the development and maintenance of secondary lymphoid organs (SLOs) and induces TLSs *de novo* in cancer. The co-expression profile of LIGHT with TLS signature indicates its great potential in the formation of TLSs in Immunity_H clusters (Figure 1D). Furthermore, high expression of CXCL13 (TLS signature) correlated with better 5 year survival in PRAD (Figure 1E). Taken together, the high LIGHT expression correlated with not only enhanced T cell anti-tumor immunity directly but also reversed the immunosuppressive tumor microenvironment, which benefits a lot from immune cell infiltration and anti-tumor immune responses.

PSMA-CAR-T cells with LIGHT expression show improved anti-tumor immune responses

In order to confirm the advantages of LIGHT in adoptive immune cell therapy, we construct the prostate-specific membrane antigen (PSMA)-targeted CAR-T (Pbbz CAR-T) through a commonly used scFv J591[18] with or without LIGHT (Figure 2A). Generally, the full-length transmembrane LIGHT will be cleaved into a soluble form by metalloproteinase activity to influence surrounding cells to form more TLSs.[19] Therefore, we compared the LIGHT production between the soluble truncated form (LIGHTt66) and the full-length transmembrane form (LIGHT-TM) in 293T cells. Although the CAR-positive rate is almost the same in LIGHTt66- and LIGHT-TM-expressing 293T cells (Figure 2B), the secretion of LIGHT in LIGHTt66 is much higher than the LIGHT-TM in 293T cells (Figure 2C). Although they have similar killing activity when overexpressed in CAR-T (Figure S1A), we chose LIGHTt66, which has cross-species bioactivity in both human and mouse with stable and higher affinity as well as paracrine function, for further study.[20] Subsequently, both PSMA CAR (Figure 2D) and LIGHT (Figure 2E) are highly expressed in PSMA-CAR T cells. As the VTP RGR has been found to be capable of specifically targeting tumor tissues through receptors that are expressed in abnormal blood vessels, we found co-localization of RGR receptor platelet-derived growth factor receptor β (PDGFRβ) with CD31 angiogenic marker in metastasized human prostate cancer tissues (Figure S1B).[21] Furthermore, we observed that RGR co-localized with CD31 in C42 tumors (Figure S1C). Accordingly, in order to specifically deliver LIGHT in tumor tissues, we fused the well-studied VTP RGR[22,23] with the C terminus of hmLIGHTt66 (LV) and co-expressed it in Pbbz CAR-T (Pbbz-LV CAR-T). Pbbz-LV CAR-T cells displayed significantly increased proliferation (Figure 2F) and cytotoxicity (Figure 2G) compared with Pbbz CAR-T cells, which is consistent with the function of HVEM.[24,25] Meanwhile, significant LIGHT secretion as well as enhanced interferon γ (IFN-γ) and TNF-α production induced by PSMA-expressed PC3 cells were observed in Pbbz-LV CAR-T cells

Figure 1. LIGHT is a potential modulator to induce TLSs and increase tumor infiltration

(A) Hierarchical clustering of prostate cancer (PRAD) and the enrichment levels of 29 immune-related cells and types in the high immune cell infiltration group (Immunity_H), the middle immune cell infiltration group (Immunity_M), and the low immune cell infiltration group (Immunity_L). The tumor purity, ESTIMATE score, immune score, and stromal score of every patient gene were calculated by ESTIMATE's algorithm. (B) The expression of nine-gene TLS signature and TNFSF14/LIGHT in trichotomized subtypes. (C) Spearman's correlation analysis between the expression levels of TNFSF14 and ESITIMATE score in human PRAD TCGA samples (Spearman's correlation analysis, $r = 0.55$; $p < 0.001$). (D) LIGHT expression in high (green), middle (blue), and low (red) immune cell infiltration subtypes (ANOVA test). (E) TLS signature (CXCL13) Kaplan-Meier overall survival ($p = 0.12$) and 5 year survival rate ($p = 0.0093$) of prostate cancer.

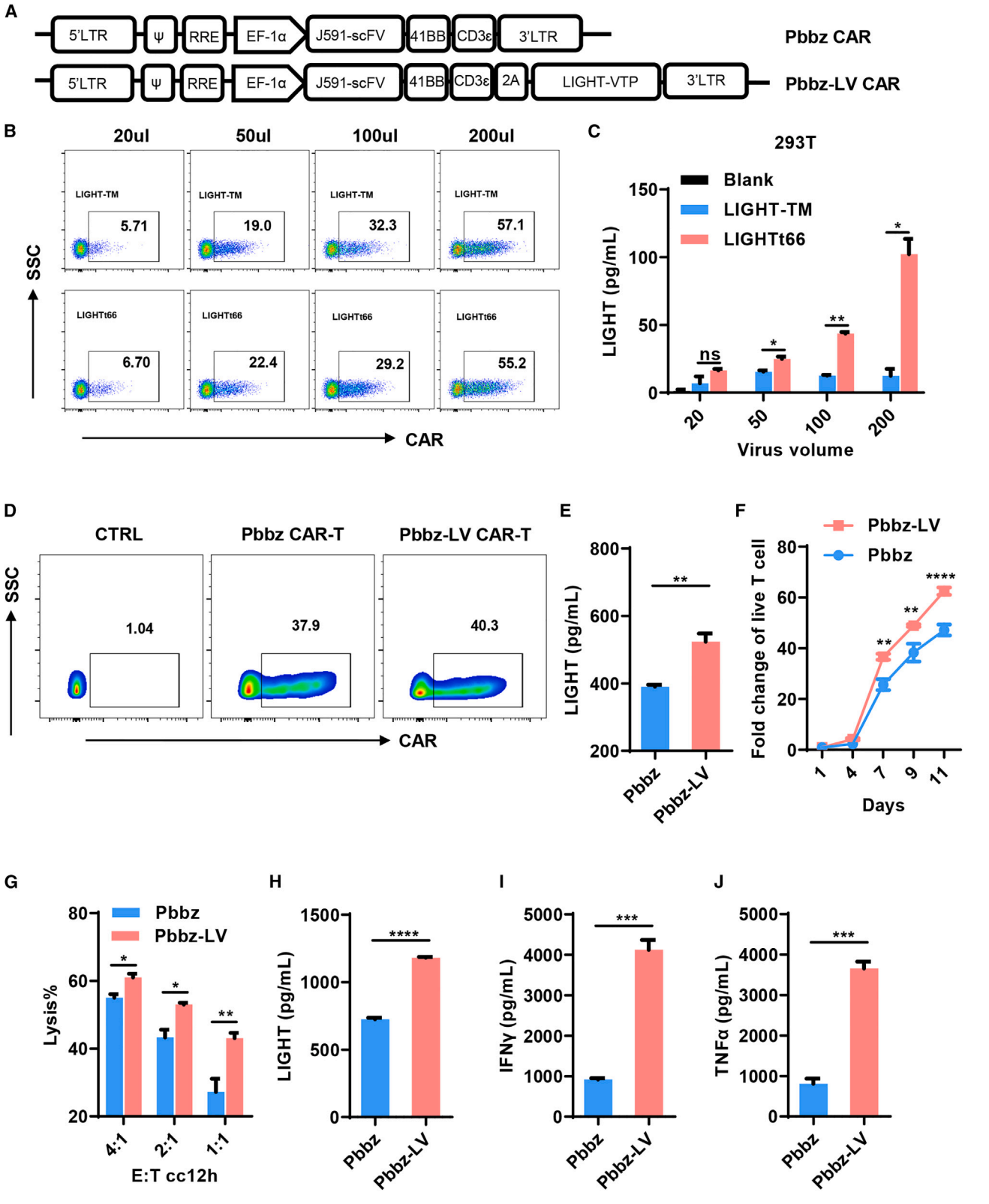

(legend on next page)

(Figures 2H–2J). Collectively, our findings demonstrated that cytotoxicity, expansion, and cytokine releasing are all enhanced obviously in Pbbz-LV CAR-T cells.

LTβR-associated chemokines and adhesion molecules are induced by Pbbz-LV CAR-T cells

It has been reported that LTβR activated the expression of chemokine CCL21, CCL19, CXCL13, and adhesion molecule VCAM-1.[26] To further confirm that the function of Pbbz-LV CAR-T cells is enhanced in an LTβR-dependent manner, we detected the expression of CCL19 in patient-derived stromal cancer-associated fibroblast (CAF) cells and showed that recombinant hLIGHT (human LIGHT) obviously increased CCL19 expression at both the mRNA (Figure 3A) and protein levels (Figure 3B). Similar data were also observed in recombinant soluble hLIGHT-treated tumor cells (Figure 3C). Moreover, in view of the negative role of abnormal vasculature and stromal cells in shaping the prostate cancer microenvironment, we injected mLIGHT (murine LIGHT) intratumorally in PC3 xenograft mouse prostate tumor models. As expected, murine CCL19 was also upregulated significantly by mLIGHT *in vivo* (Figure 3D). Next, we stimulated CAF cells and PC3 cells with supernatant from different CAR-T cells. Interestingly, the supernatant from Pbbz-LV CAR-T cells significantly upregulated CCL19, CCL21, and CXCL13 expression on CAF (Figure 3E) and PC3 (Figure 3F) cells, which are all critical chemoattractants for T cells, DCs, and other immune cells to neoplastic sites.[27–29] Meanwhile, the recombinant hLIGHT also increased the expression of CCL19, CCL21, and VCAM-1 in human umbilical vein endothelial cells (HUVECs) (Figure 3G). Accordingly, Pbbz-LV CAR-T cells show more adherence to HUVECs following 24 h incubation (Figure 3H), and enhanced CCL19, CCL21, and CXCL13 expression was observed in murine bone marrow cells after stimulation by mLIGHT (Figure 3I) and supernatant of CAR-T cells (Figure 3J), suggesting the secreted LIGHT has great potential to initiate chemotaxis in bone metastases. Taken together, the supernatant from Pbbz-LV CAR-T cells plays key roles in reconstituting the high immune-infiltrating tumor microenvironment through inducing TLS-associated chemokines in both stromal cells and cancer cells.

Supernatant from Pbbz-LV CAR-T cells enhance immune cell recruitment

As CCL19, CCL21, and CXCL13 increased by Pbbz-LV CAR-T cells are all critical for the formation of SLOs and TLSs in the tumor microenvironment, we performed Transwell migration assays to appraise the potential of Pbbz-LV CAR-T cells in recruiting immune cells (Figure 4A). Migration of responder T cells to PC3 and CAF was significantly enhanced by recombinant LIGHT stimulation (Figures 4B and 4C), while LIGHT did not exhibit attraction for T cells alone (Figure 4D), which is consistent with enhanced chemokine production. Moreover, the supernatant from Pbbz-LV CAR-T cells recruits more T cells than Pbbz CAR-T cells through activating PC3 (Figure 4E), CAF (Figure 4F), and bone marrow (BM) cells (Figure 4G), suggesting that LIGHT recruits T cells through activating surrounding cells. Furthermore, both recombinant LIGHT and the supernatant of Pbbz-LV CAR-T cells increased CAR-T cell recruitment and cytotoxicity to the PC3 cancer cells obviously (Figures 4H–4J). Taken together, these data suggested that the cytotoxicity of Pbbz-LV CAR-T benefits a lot from immune cell recruitment.

Pbbz-LV CAR-T cells exhibit signature enrichment for IFN-γ and inflammation response genes

Then, RNA-seq analysis was performed to explore the influenced signaling pathway in Pbbz-LV CAR-T cells. As shown in Figure 5A, a lot of genes were upregulated in Pbbz-LV CAR-T cells, including LIGHT, T cell activation-related cytokines (IL-13, IFNG, IL-2), and genes facilitating T cell survival and proliferation (IL-9, IL-12A, IL-18, BCL6), and these data were further confirmed by quantitative real-time PCR (Figures 5B–5I). Previous studies showed that IFN-γ dramatically enhances LIGHT-mediated apoptosis of cancer cells,[24] which is consistent with superior tumor lytic activity and enhanced IFN-γ secretion. In addition, GSEA showed a significant enrichment of genes upregulated in response to IFN-γ (Figures 5J and S2A), suggesting that elevated IFN-γ activity synergizes with LIGHT to increase tumor-lytic potential. Furthermore, we observed an enrichment of genes within the TNF-α, which is in line with the data of ELISAs (Figures 5K and S2B). In addition, enriched IL-2/STAT5 signaling was also found in Pbbz-LV CAR-T cells (Figures 5L and S2C), which implied that Pbbz-LV CAR-T cells have remarkable cell activation and proliferation. Interestingly, we also observed that some inflammatory genes were upregulated in Pbbz-LV CAR-T cells, such as IL-18 and BCL6, which promotes T cell survival and inhibits T cell apoptosis (Figures 5M and S2D). Furthermore, we observed an enrichment of hallmark genes of the G2M checkpoint (Figures S2E and S2F), suggesting that LIGHT promoted cell-cycle progression

Figure 2. Functional engineering of the secreted LIGHT-VTP in T cells

(A) Schematic representation of the CAR-expressing lentiviral vector constructs of Pbbz CAR (top) and Pbbz-LV CAR (LV: LIGHT-VTP; bottom), a truncated sequence of the full-length LIGHT (cross-species bioactivity in both human and mouse), lacking the cytoplasmic and transmembrane domains, which infused with VTP was linked by 2A with PSMA-specific fusion receptor that encompasses an scFv derived from the J591 antibody. (B and C) Filtered lentiviral supernatants of LIGHT-TM (full-length LIGHT) CAR and LIGHTt66 (soluble truncated LIGHT) CAR were added to 293T cells in different volumes, CAR expression was detected after 48 h infection (B), and supernatants of those cells were used to measure LIGHT by ELISA (C). Untransfected 293T cells (blank) were used as a negative control. (D) CAR expression of CAR-T cells after 48 h infected with relative virus and untransfected T cells as a control (CTRL). (E) LIGHT expression in supernatants of CAR-T cells after 48 h infection. (F) Fold change of absolute numbers of viable Pbbz CAR-T and Pbbz-LV CAR-T cells on different days. Relative to day 1 with a total of 1×10^5 CAR-T cells. Data represent the mean ± SEM of triplicate values. (G) Cytotoxicity assay using PC3-PSMA$^+$ cells as targets. Target cells were co-cultured with Pbbz CAR-T or Pbbz-LV CAR-T cells at the indicated effector/target (E/T) ratios for 12 h. Data represent the mean ± SEM of triplicate wells. (H–J) After co-culturing Pbbz CAR-T or Pbbz-LV CAR-T cells with PC3-PSMA$^+$ cells at an E:T ratio of 2:1 for 24 h (target cells: 0.5 M, 1.5 mL), the concentrations of LIGHT (H), IFN-γ (I), and TNF-α (J) in supernatants were measured by ELISA kits. All error bars represent mean ± SEM. $^*p < 0.05$, $^{**}p < 0.01$, $^{***}p < 0.001$.

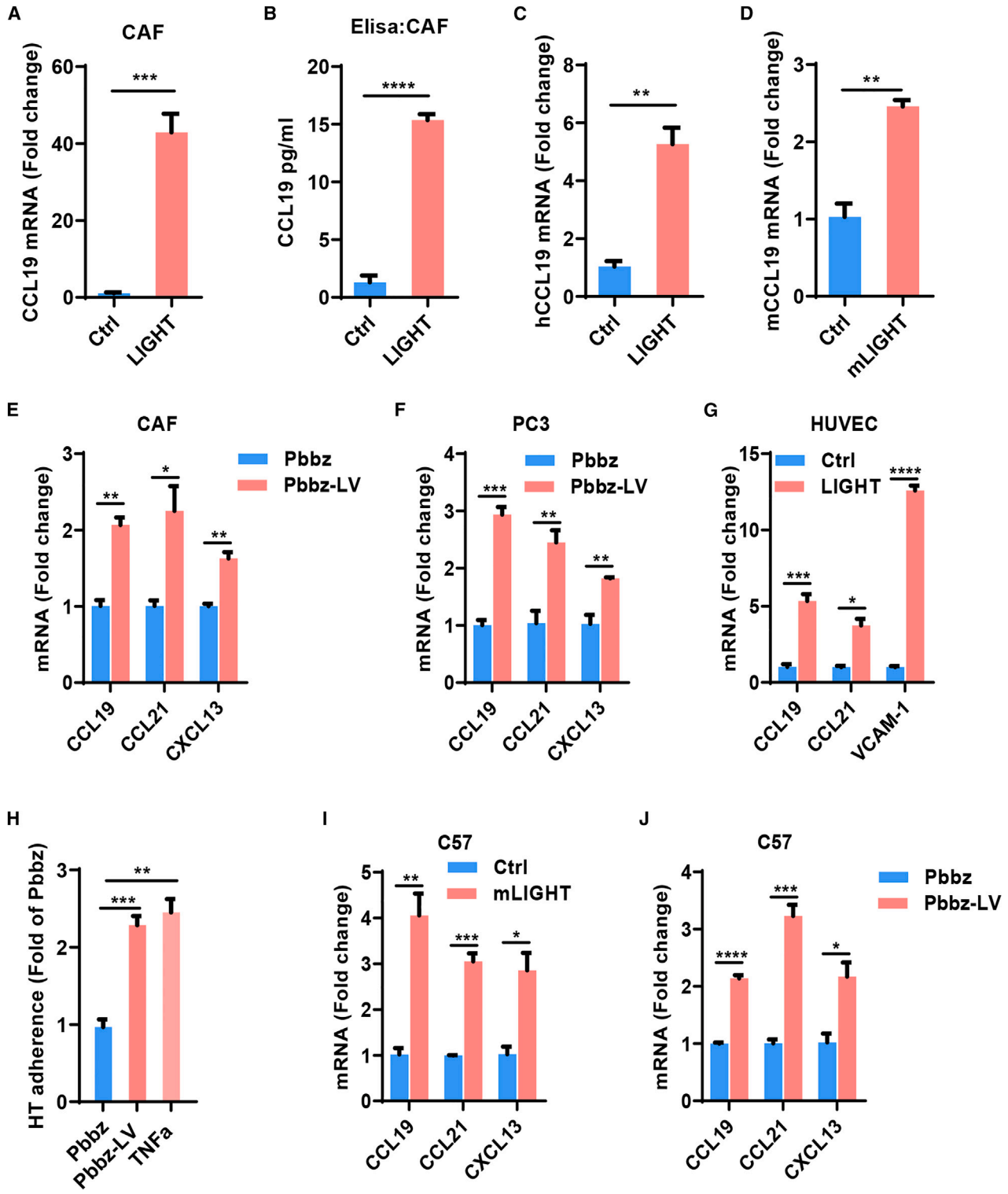

Figure 3. LIGHT induces a specific inflammatory transcriptomic profile

(A) mRNA fold increase of CCL19 in CAF cells stimulated with recombinant human LIGHT protein (100 ng/mL) for 24 h. (B) CAF cells were stimulated with recombinant human LIGHT protein (100 ng/mL) for 24 h, and CCL19 in supernatants was measured by ELISA. (C and D) CCL19 mRNA expression was quantitatively analyzed in PC3 subcutaneous NSG mice after 1 week of intratumoral treatment with recombinant human LIGHT or mLIGHT (10 ng/day) in comparison to PBS-treated tumors. hCCL19, human

(legend continued on next page)

and proliferation of Pbbz-LV CAR-T cells. Overall, these data highlight LIGHT as a multifunction regulator to increase the expansion, differentiation, and immune activity of T cells.

Enhanced anti-tumor activity of Pbbz-LV CAR-T cells in subcutaneous and metastasis tumor models

Enhanced immune cells recruiting by supernatant from Pbbz-LV CAR-T cells encouraged us to further assess potency of it in xenograft tumor models (Figure 6A). Therefore, we compared Pbbz-LV CAR-T with Pbbz CAR-T in NSG mice bearing PC3-PSMA$^+$ tumors. As shown in Figure 6B, the adoptive transfer of Pbbz-LV CAR-T cells exhibits faster kinetics in tumor clearance on day 9 and induced complete regression of tumors on day 15. Accordingly, significantly prolonged survival was also observed in Pbbz-LV CAR-T cells (Figure 6C). Immunofluorescence staining assay revealed that Pbbz-LV CAR-T cells have much more tumor infiltration and a high level of CCL21 expression in tumor tissues (Figure 6D). Then, we assessed whether Pbbz-LV CAR-T cells drive inflammatory toxicities in the NSG mice model, but serum cytokines were little changed between the Pbbz-LV and Pbbz groups (Figures S3A–S3E). We also investigated the potential histological abnormalities in T cells of Pbbz CAR-T- and Pbbz-LV CAR-T-treated mice; no evident lesions were observed in tissue sections from each group (Figure 6E). According to our findings, supernatant from Pbbz-LV CAR-T cells promotes the expression of chemokines such as CCL19 and CCL21 in BM cells, and thus we assessed Pbbz-LV CAR-T cells in a prostate cancer bone metastasis model (Figure 6F). As shown in Figures 6G and 6H, mice treated with Pbbz-LV CAR-T cells have more rapid complete remission and prolonged survival time. In conclusion, Pbbz-LV CAR-T cells could be a promising approach to treat local and advanced prostate cancer through augmenting immune cell infiltration and migration to the tumor microenvironment.

LIGHT-OT-1 T cells normalize blood vessels and enforce intratumoral lymphoid structures

In order to further investigate the potential of LIGHT in normalizing tumor vessels and TLS induction, we constructed OT-1 T cells overexpressing hmLIGHT (Figures S4A–S4C). We transferred OT-1 T cells with or without LIGHT expression to syngeneic B16F10-OVA melanoma tumor models. Consistent with above data, mice treated with LIGHT-OT-1 T cells showed superior tumor control (Figure 7A) and prolonged survival time (Figure 7B), whereas the body weight of these mice was little affected (Figure 7C). Meanwhile, both the percentage of T cells and NK cells (Figures 7D and S4D) and tumor infiltration (Figures 7E and 7G) were enhanced significantly in LIGHT-OT-1 cell-infused mice. Furthermore, the proportion of infiltrating regulatory T (Treg) cells was little changed (Figure 7F), but CD62L$^+$CD44$^+$ memory T cells were enhanced in the LIGHT-OT-1 treatment group (Figures S4E and S4F), and T cell exhaustion markers such as PD-1 and TIGIT were similar in each group (Figures S4G–S4J). Furthermore, T cells, DCs, B cells, myeloid cells, and tumor-associated and normalized vascular high endothelial venules within tumors were all co-localized significantly in LIGHT-OT-1 cell-treated mice (Figure 7H), suggesting that more TLS-like structures were reconstituted by LIGHT. Consistent with above data, LIGHT engagement facilitated the induction of *ccl19* (Figure 7I), *ccl21* (Figure 7J), and *cxcl13* (Figure 7K) in tumors. In addition, the production of inflammatory cytokines IL-1β, IL-6, and LIGHT (Figures S4K–S4M) and the AST/ALT ratio (Figure S4N) were little changed in the LIGHT C57BL/6 mouse model. In summary, our findings indicate that normalized tumor vessels and chemotactic mediators enhanced DC, NK cell, T cell, and other innate immune cell infiltration, thus participating in the synergistic anti-tumor effect of LIGHT.

DISCUSSION

The penetration and infiltration of immune cells into solid tumors is considered the biggest obstacle in cancer immune therapy. Thus, reconstitution of a more favorable tumor microenvironment for immune cell infiltration has been demonstrated to augment long-term survival rates and elicit favorable responses to immune therapy. Among them, heterogeneous expression of chemokines has been widely used to improve the outcome of adoptive cellular immunotherapy, whereas chemokine induction seems not to be strong enough for cold tumors such as prostate cancer for the poor ectopic lymphoid aggregates in tumor tissues. Thus, it is crucial to establish a method to generate efficient "armed" CAR-T cells to increase their and other immune cells trafficking to solid tumors to enhance the therapeutic effect. In this study, we demonstrated that LIGHT-expressing CAR-T cells not only enhanced the production of chemokines but also facilitated the formation of TLSs for immune cell infiltration. Furthermore, engineered LIGHT CAR-T cells showed superior anti-tumor efficacy in both immunodeficient NSG and wild-type C57BL/6 xenograft tumor mouse models, suggesting that LIGHT expression has great potential to expand the application of CAR-T therapy in solid tumor.

Cold tumors are characterized by the lack of T cell infiltration in the tumor bed, not only because of a lack of appropriate chemokines but also because they are restricted by the tumor vasculature and lymphoid structure formation. After retrieving RNA-seq data from TCGA database, TLS signature genes present as positive prognostic

CCL19; mCCL19, mouse CCL19. (E) mRNA fold increase of the indicated molecules in CAF cells stimulated for 24 h with supernatants of CAR-T cells. (F) mRNA fold increase of the indicated molecules in PC3 cells stimulated for 24 h with supernatants of CAR-T cells. (G) mRNA fold increase of the indicated molecules in HUVECs (human umbilical vein endothelial cells) stimulated for 24 h with recombinant human LIGHT protein (100 ng/mL). (H) Human T (HT) cell adhesion to HUVECs, HUVECs pre-incubated in indicated supernatants from CAR-T cells, or TNF-α protein for 24 h prior to add CFSE-labeled T cells, and adhering T cells were counted by flow cytometry after 20 h. TNF-α (200 ng/mL) is a positive control. (I and J) Bone marrow cells from C57BL/6 (C57) mice were stimulated with recombinant mouse LIGHT (100 ng/mL) (I) or indicated supernatants of CAR-T cells (J) for 24 h, and transcripts of indicated molecules in cells were detected by quantitative real-time PCR. Representative data are mean ± SEM from triplicate cultures from three independent experiments. $^*p < 0.05$, $^{**}p < 0.01$, $^{***}p < 0.001$. Student's t test.

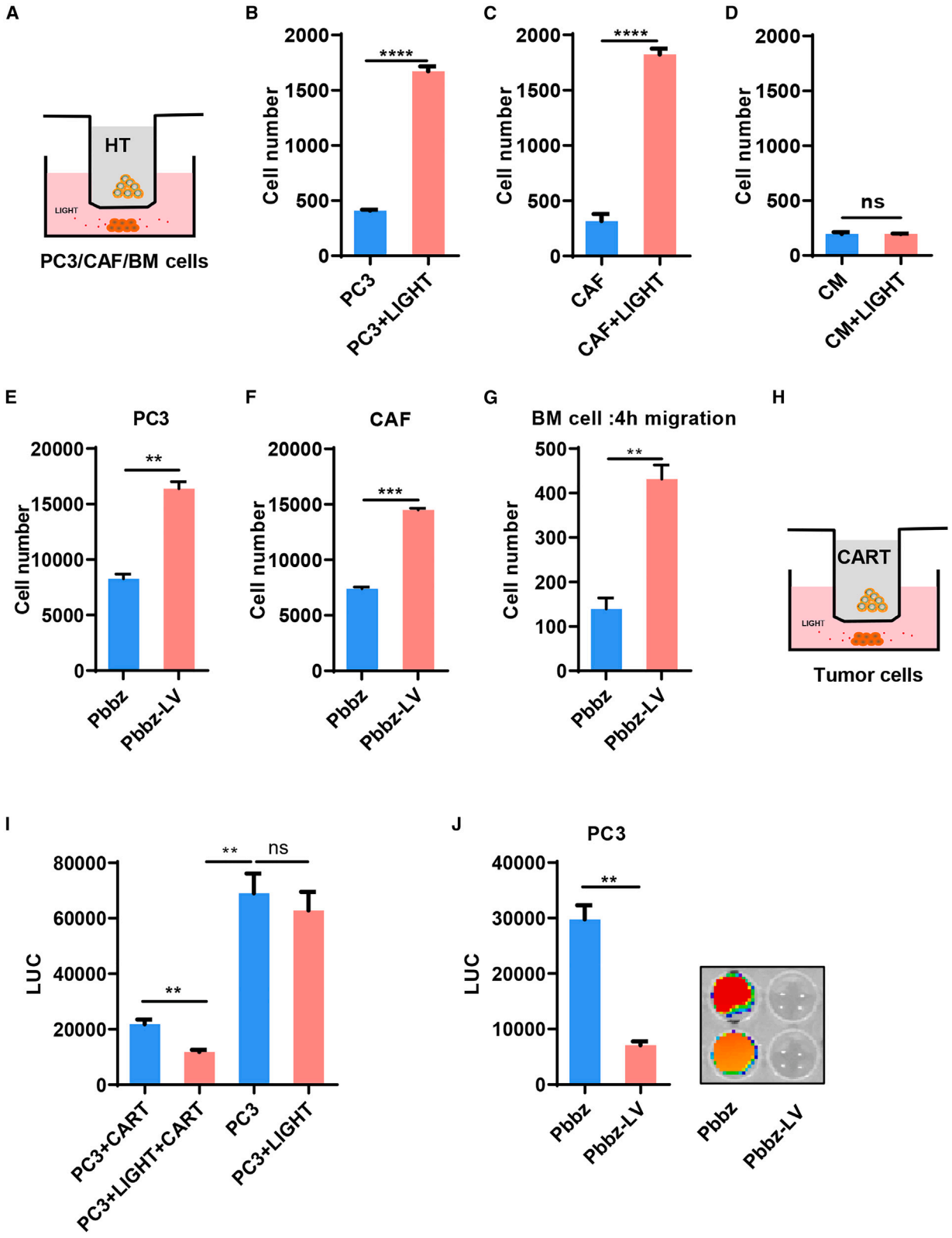

(legend on next page)

factors in most solid tumors. Among them, CCL19, CCL21, CXCL13, and LIGHT, are all TLS-promoting factors only expressed in patients with high immune infiltration, whereas infiltration signaling deficiency in cold tumors is not only mediated by one or two chemokines, but a set of chemokines and adhesion molecules that coordinate together to recruit anti-tumor immune cells were involved. Thus, single chemokine or chemokine receptor activation may not achieve a meaningful clinical response. Only facilitating the formation of a more comprehensive chemokine set that favors intratumoral vascular normalization and TLS formation could fundamentally solve the problem of CAR-T infiltration. Previous studies have shown that the CCL19/CCL21 axis recruits T and other innate immune cells through CCR7; accordingly, we observed a significant incerase of memory T cells in LIGHT CAR-T cells, whereas the Treg cells were little changed. Along with the immunosuppressive hallmark of cancer, the tumor endothelium is usually anergic, with decreased adhesion molecules, including intercellular adhesion molecule 1 (ICAM-1) and vascular cell adhesion molecule 1 (VCAM-1), that are required for leukocyte adhesion, extravasation, and subsequent tumor infiltration. Consistent with reported function in facilitating ICAM-1 and VCAM-1 expression in tumor vessels,[30] LIGHT co-expressing CAR-T cells adhere more to the vessel wall and further induce normalization of abnormal blood vessels in tumors to generate $MECA79^+$ HEV, which is key structure for immune cell entry into tissues. Here, we demonstrated that LIGHT not only facilitated T cell-mediated cytotoxicity directly but also mobilized all available forces from bystander cells to express CCL19 and CCL21, which integrated two kinds of chemokines' functions and maintained the advantages of promoting CAR-T cell killing, a proliferation effect to optimize the outcome of cancer immune therapy.

While antibody-drug conjugates (ADCs) are designed to selectively deliver the ultratoxic payload directly to target cells, we can also see CAR-T function as a micropharmacy of living cells with continuous LIGHT secretion that have much longer half-life than intravenously administrated cytokines and alter the immune milieu of solid tumors. On the other hand, LIGHT is an initiator of T cell co-stimulation signals regulating T cell immune responses by the HVEM; it stimulates survival, proliferation, and cytokine production in T cells by the activation of the nuclear factor κB (NF-κB) pathway. Based on our *in vitro* experiments and sequencing data, engagement of LIGHT in CAR-T cells is implicated in enhanced cytotoxicity and expansion. Loss of the IFN-γ pathway in tumors has been reported as a novel mechanism of tumor resistance to CAR-T killing.[31] After comparing the RNA-seq data from Pbbz and Pbbz-LV CAR-T cells, a significant increase of IFN-γ, IL-9, IL-12A, and IL-18 secretion was observed in Pbbz-LV CAR-T cells, suggesting the great potential of Pbbz-LV CAR-T cells in fighting against tumor-intrinsic resistance.

In conclusion, we evaluated the potency of Pbbz-LV CAR-T in solid tumor therapy through activating and recruiting CAR-T cells as well as endogenous immune cells. We demonstrated that the secreted LIGHT normalized tumor vasculature to facilitate immune cell infiltration and T cell-mediated anti-tumor responses, which suggested that Pbbz-LV CAR-T cells have great potential in reshaping immunosuppressive microenvironments to overcome cancer resistance against adoptive cell therapy.

MATERIALS AND METHODS

Mice

Only male mice were obtained in this study, and the age at which animal models are commonly used is 6–8 weeks. NSG (NOD/SCID/IL-2RG) mice were purchased from GemPharmatech. C57BL/6 mice were provided by the animal center of East China Normal University, and OT-1 mice were purchased from the Jackson Laboratory. All mice were housed in specific pathogen-free conditions in the animal center of East China Normal University. All mouse experiments were performed in accordance with national guidelines for the humane treatment of animals (national animal treatment rules), and protocols were approved by the East China Normal University Ethics Committee (ethical approval number m20210602).

Cell lines and culture condition

Peripheral blood for CAR-T cells was obtained from healthy volunteers (n = 3 or more), and informed written consent of all participants were obtained. All blood samples were collected and handled according to the ethical and safety procedures approved by the Clinical Ethics Committee of the First Affiliated Hospital, College of Medicine, Zhejiang University (IIT20210001C-R1 for human subjects). Lymphocyte separation medium (TBD Science, LTS10770015) was applied to obtain peripheral blood mononuclear cells (PBMCs), which were further treated with CD4/CD8 MACS (Miltenyi) to get $CD4^+/CD8^+$ T cells. After 2 days of activation with the CD3 and CD28 compound, T cells were used to conduct

Figure 4. LIGHT promotes CAR-T cell migration to the tumor microenvironment (TME) in a paracrine manner

(A) Schematic diagram of T cell migration model. Cell culture supernatants of CAR-T cells were collected at 48 h; PC3 or CAF cells were cultured in the lower chamber pre-stimulated with indicated supernatants or recombinant human LIGHT protein for 24 h; CFSE pre-stained HT cells were added in the upper chamber (5 μm Transwell); and migrated cells was assessed by flow cytometry after 4 h. (B–D) Recombinant human LIGHT protein induces the migration of T cells to PC3 cells (B) and CAF cells (C); migrated cell number is shown; and LIGHT protein itself does not induce migration (D). CM, culture medium. (E) Pbbz-LV supernatant induces the migration of T cells to PC3 cells, and the migrated cell number is shown. (F) Pbbz-LV supernatant induces the migration of T cells to CAF cells, and the migrated cell number is shown. (G) Bone marrow cells from C57BL/6 mice cultured in the lower chamber were pre-stimulated with indicated supernatants for 24 h, then CFSE pre-stained mouse T cells were added in the upper chamber (5 μm Transwell), and migrated cells were assessed by flow cytometry after 4 h. (H–J) Schematic diagram of migration and kill assay (H). PC3-$PSMA^+$ cells were seeded in the lower chamber and pre-stimulated with recombinant human LIGHT (I) (100 ng/mL) or indicated supernatants (J) for 24 h, and Pbbz CAR-T cells were added in the upper chamber. Cytotoxicity was determined by luciferase (LUC value), and IVIS picture was shown after 20 h. All data with error bars represent the mean ± SEM of triplicate values, p values were calculated by unpaired Student's t test, and one representative data from three independent experiments are shown. $^*p < 0.05$, $^{**}p < 0.01$, $^{***}p < 0.001$.

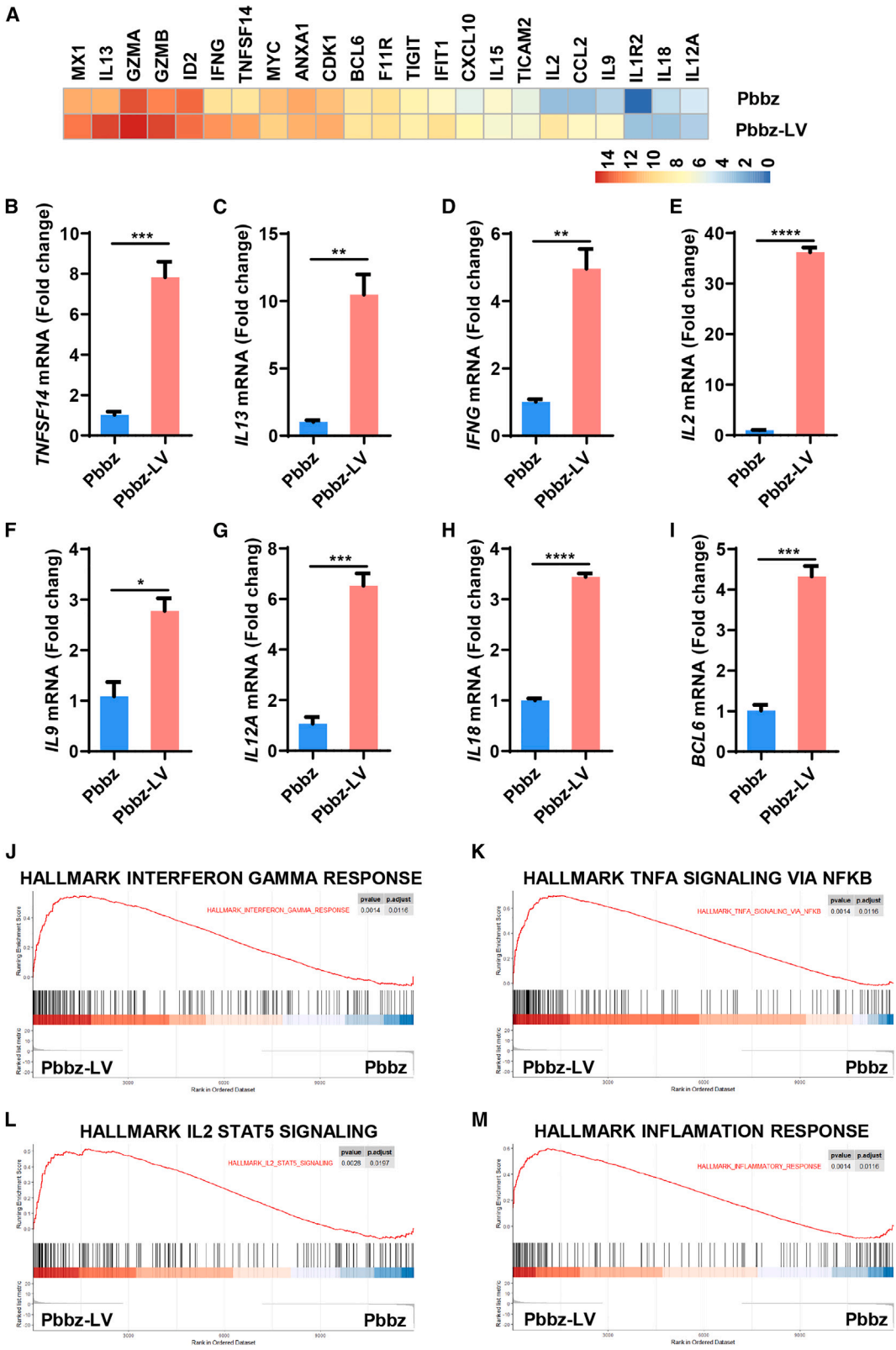

(legend on next page)

the experiment. Prostate cancer cell line PC3 and C42 cells were bought from the American Type Culture Collection (ATCC). PC3 cells were cultured in DMEM medium (Gibco) supplemented with 10% FBS and 1% P/S (100 U/mL penicillin and 100 mg/mL streptomycin). C42 cells were cultured in RPMI 1640 (Gibco) supplemented with 10% FBS and 1% P/S. PSMA was overexpressed in PC3 cells by lentivirus, and then the cells were screened with puromycin dihydrochloride (2–4 μg/mL; BBI Life Science, F118BA0026) for stable overexpression of PSMA and luciferase. Primary prostatic CAF cells were provided by Changhai Hospital (Shanghai, China), and the passage number of stromal cells used in this work was limited to 3–10. The cell line HUVECs (PCS-100-013), 293T cells, and B16F10 were obtained from ATCC, and B16F10-OVA was constructed by lentivirus and sorted by flow cytometry. All cells were maintained in DMEM complete medium in a humidified atmosphere containing 5% carbon dioxide (CO_2) incubators (Thermo Scientific) at 37°C.

Plasmid construction

We constructed a second-generation CAR. The first nucleic acid sequence of the CAR comprised of the anti-human PSMA-scfv (J591) linked in frame to the hinge and transmembrane regions of the human CD8α chain and intracellular human 4-1BB (CD137) and CD3ζ signaling domains and was transferred to the plasmid empty vector (lentiviral transfer vector pELPS) using Xba I and Sal I double enzymatic digestion. Further, vectors were connected a second nucleic acid sequence that included a secretory signal peptide (SP), hmLIGHTt66 (truncation of the N-terminal 65 amino acids, no cytoplasmic and transmembrane domains), or full-length hmLIGHT, VTP (RGR: GGGCRGRR STG) with the first nucleic acid sequence, by a P2A peptide sequence to intercalate among the two sequences. Thus, we obtained pELPS-Pbbz plasmid including only the first nucleic acid sequence and pELPS-Pbbz-LV plasmid including both of these two sequences.

To match the mouse system, we also designed a second recombinant retroviral vector based on mouse stem cell virus-based splice-gag vector (MSGV) retroviral backbone. We cloned genes for soluble hmLIGHTt66-VTP and Thy1.1 marker into the MSGV retroviral backbone to produce the MSGV-Thy1.1-P2A-hmLIGHTt66-VTP vector. As control, we used an empty vector containing Thy1.1. All of these sequences were synthesized by GenScript.

Retrovirus and lentivirus preparation of CAR-T cells

For lentivirus production, 293T cells were used to produce lentivirus that carried CAR. 293T cells were cultured to a degree of 80%–90% and co-transfected with three-plasmid system (packaging vectors psPAX2, envelope plasmid pMD2.G, and CAR plasmid) by using polyethyleneimine (Polysciences, PEI MAX 40000). Renewed medium after 6–8 h of post-transfection and virus-containing supernatant was harvested and concentrated. Further, viral supernatants generated were serial diluted, and then T cells were infected by the lentivirus, which mixed evenly with Polybrene at MOI = 10. The expression of CAR was analyzed after 2 or 3 days, and the CAR-T cells were used for further experiments.

We used retrovirus as the vector to prepare viruses that infect mouse T cells. 293T cells were transfected with the MSGV-Thy1.1-P2A-hmLIGHTt66-VTP or control plasmid together with the retroviral packaging plasmid Pcl-Eco (Addgene) by using polyethyleneimine. Retroviral supernatant was collected 2 days later. Murine T cells isolated (Miltenyi) from fresh spleen of healthy OT-1 mice were stimulated with anti-mouse CD3/CD28 magnetic beads (Gibco) for 48 h and then infected with retrovirus in RetroNectin (Takara)-coated plates.

Cytotoxicity assay

Cytotoxicity of CAR-T cells was determined by luciferase-based killing assay. 2×10^4 PC3-PSMA$^+$ target tumor cells expressing firefly luciferase were co-cultured with different types of CAR-T cells at varying effector-to-target ratios in triplicate in 96-well plates (Corning) in a total volume of 100 μL cell media. 12 h later, 10 μL fluorescein substrate (Invitrogen) was added per well, and luminescence was measured using a microplate reader (BMG LABTECH SPECTROstarNano, 562 nm) and IVIS instrument (IVIS Lumina III). The percentage of lysis was determined by a standard curve by linear regression of luminescence against a viable number of PC3-PSMA$^+$ cells.

Flow cytometry

Cells were stained with fluorochrome-conjugated antibodies against markers shown in Table S1 according to the manufacturer's

Figure 5. Pbbz-LV CAR-T cells induced pro-inflammatory cytokines and enhanced anti-tumor signatures

(A) Heatmap of representative differentially expressed genes between Pbbz CAR-T cells and Pbbz-LV CAR-T cells. Heatmap generated using the R-package pheatmap. (B–I) Representative differentially expressed genes validated using quantitative real-time PCR. TNFSF14 (B) and IL-13 (C), IFN-γ (D), IL-2 (E), IL-9 (F), IL-12A (G), IL-18 (H), and BCL6 (I) were upregulated, and data are shown as the mean ± SEM of the fold change in gene expression for Pbbz-LV CAR-T cells versus Pbbz CAR-T cells. (J) GSEA for the expression profiles of Pbbz-LV CAR-T cells compared with Pbbz CAR-T cells using HALLMARK_INTERFERON_GAMMA_RESPONSE gene sets (https://www.gsea-msigdb.org/gsea/msigdb/cards/HALLMARK_INTERFERON_GAMMA_RESPONSE). (K) GSEA for the expression profiles of Pbbz-LV CAR-T cells compared with Pbbz CAR-T cells using HALLMARK_TNFA_SIGNALING_VIA_NFKB gene sets (https://www.gsea-msigdb.org/gsea/msigdb/cards/HALLMARK_TNFA_SIGNALING_VIA_NFKB). (L) GSEA for the expression profiles of Pbbz-LV CAR-T cells copompared with Pbbz CAR-T cells using HALLMARK_IL2_STAT5_SIGNALING gene sets (https://www.gsea-msigdb.org/gsea/msigdb/cards/HALLMARK_IL2_STAT5_SIGNALING). (M) GSEA for the expression profiles of Pbbz-LV CAR-T cells compared with Pbbz CAR-T cells using HALLMARK_INFLAMMATORY_RESPONSE gene sets (https://www.gsea-msigdb.org/gsea/msigdb/cards/HALLMARK_INFLAMMATORY_RESPONSE). Quantitative real-time PCR error bars represent the mean ± SEM of triplicate values, and p values were calculated by unpaired Student's t test. *$p < 0.05$, **$p < 0.01$, ***$p < 0.001$.

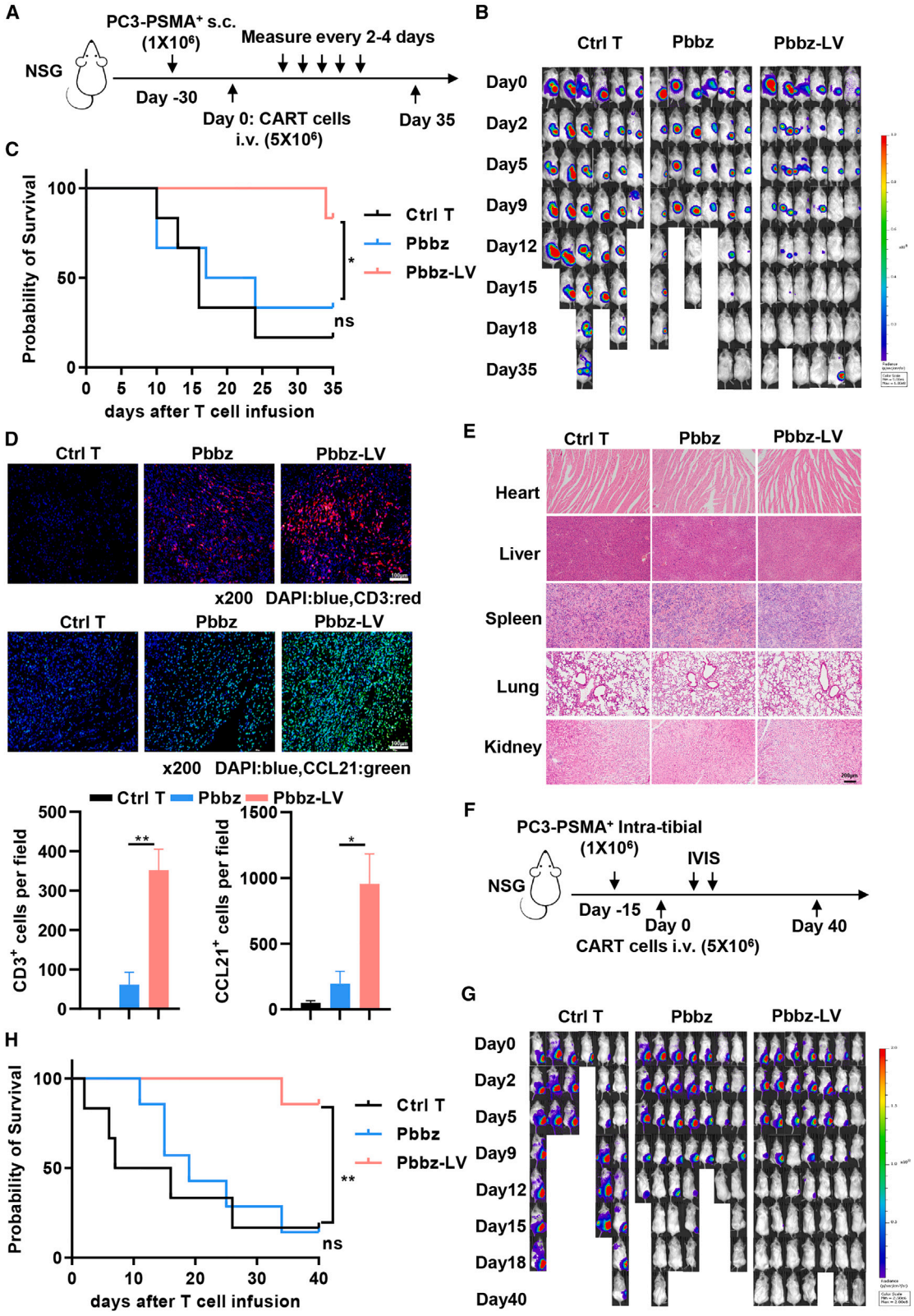

(legend on next page)

instructions. Flow cytometry was performed on the Fortessa-LSR II cytometer (Becton-Dickinson) and analyzed with FlowJo X 10.0.7r2 (Tree Star). Cytokines in murine serum were detected by CBA Flex Set (BD Pharmingen) and analyzed by FCAP Array software.

ELISA and quantitative real-time PCR

LIGHT/TNFSF14, IFN-γ, TNF-α, and CCL19 were measured by human LIGHT/TNFSF14 (R&D, DY664), mouse TNFSF14 (Signalway Antibody, EK6202), human IFN-γ (Invitrogen, 88-7316-88), human TNF-α (Invitrogen, 88-7346-88), and human CCL19 (R&D, DY361) ELISA kits following the manufacturer's instructions, respectively. mRNA was isolated from indicated cells or tissues using an RNA extraction kit according to the manufacturer's instructions (Magen, R4801-02), and mRNA was reverse transcribed and used as template for quantitative real-time PCR. Primer sequences used for quantitative real-time PCR analysis in this study are listed in Table S2. AST/ALT was detected by the Aspartate Aminotransferase Assay Kit and the Alanine Aminotransferase Assay Kit (Nanjing Jiancheng Bioengineering Institute).

Cell adhesion assay

HUVECs grown in 24-well plates were pre-incubated with supernatants from CAR-T cells or TNF-α (SinoBiological, 10602-H01H) protein (200 ng/mL) for 24 h and then washed twice with PBS. CFSE-labeled human T cells were added to the HUVEC monolayer and incubated for 20 h. Non-adherent cells were removed from the plate by gentle washing with PBS, and the number of adherent cells was determined by flow cytometer.

Migration and migration and kill assay

The T cell migration assay was performed by using a polycarbonate filter of 5 μm pore size in 24-well Transwell chambers (Corning). Cell culture supernatants of CAR-T (Pbbz CAR-T or Pbbz-LV CAR-T) cells were collected at 48 h, and cells cultured in the lower chamber were pre-stimulated with collected supernatants or 100 ng/mL LIGHT protein (SinoBiological, 10386-H07H) for 24 h. Transwell membrane was plated carefully into 24-well plate, and CFSE pre-stained human T (HT) cells in the media were put in the upper chamber. After 3–5 h, the cells that migrated to the lower chamber were assessed by flow cytometry (Precision Count Beads, BioLegend, 424902).

In the CAR-T cell migration and kill assay, 1×10^5 PC3-PSMA$^+$ cells were cultured in the lower chamber in an ultralow attachment plate (Corning) and pre-stimulated with collected CAR-T supernatants or LIGHT protein (100 ng/mL) for 24 h, and 4×10^5 Pbbz CAR-T cells were plated into the upper chambers of 24-well Transwell plates. The cells in the lower chamber were collected after 18–24 h. The migration and cytotoxicity of Pbbz CAR-T cells were displayed by bioluminescence quantification and image analysis.

Treatment of tumor-bearing mice

Subcutaneous xenograft model: we used the immunodeficient NSG mice for the xenograft studies. To obtain prostate cancer mice model, each male NSG mouse (6–8 weeks old) was injected subcutaneously with 1×10^6 human PC3-PSMA$^+$ cells. After 30 days of tumor model establishment, further experiments were carried out. Mice were divided into 3 groups, as the average tumor size was approximately 200 mm^3, before the corresponding treatment. Each group (Ctrl T/Pbbz CAR-T/Pbbz-LV CAR-T) was treated with same number of T cells respectively through tail vein injection (5×10^6 cells/mouse, approximately 40% CAR positive) on day 0. Recipient mice were observed daily, and tumor size was tracked by digital calipers. In addition, luminescence was detected by IVIS (PerkinElmer) twice a week, and body weight was measured twice a week. All experiments complied with current national and institutional regulations and ethical guidelines and were performed by an accredited person. In specific experiments, PC3 subcutaneous NSG mice were treated intratumorally with recombinant human LIGHT or mLIGHT (SinoBiological, 50980-M07B) for quantitative real-time PCR analysis.

Bone metastasis model: for the intratibial injection model, PC3-PSMA$^+$ cells were resuspended in PBS at the density of 1×10^6 cells/10 μL, and 10 μL cell solution was slowly injected with a 28.5G needle into the tibia using a drilling motion. After 15 days, T cells (Ctrl T/Pbbz CAR-T/Pbbz-LV CAR-T) at a dose of 5×10^6 were infused intravenously. Mice were monitored twice a week by IVIS luciferase imaging.

Subcutaneous syngeneic models: B16F10-OVA cells (5×10^5 cells per mouse) were suspended in 75 μL PBS mixed with 25 μL Matrigel (Corning) and were subcutaneously injected into the back of C57BL/6 mice (male, 6–8 weeks old). Two weeks after tumor

Figure 6. *In vivo* anti-tumor effects of Pbbz-LV CAR-T cells in pre-established xenograft solid tumor models

(A) Schematic of the subcutaneous prostate xenograft tumor model; s.c., subcutaneous; i.v., intravenous. NSG mice bearing established PC3-PSMA$^+$ tumors were i.v. treated with 5×10^6 Ctrl T cells, Pbbz CAR-T cells, and Pbbz-LV CAR-T cells separately. The IVIS Lumina II In Vivo Imaging System was used to monitor tumor growth every 2–4 days. (B and C) Representative tumor bioluminescence images (B) and survival curve of mice (C) from two independent experiments. (D) Fluorescent immunohistochemistry (IHC) images show CD3 (red) and CCL21 (green) and DAPI (blue) staining in PC3-PSMA$^+$ tumors after the administration of Ctrl T cells, Pbbz CAR-T cells, or Pbbz-LV CAR-T cells on day 9, when there was a significant therapeutic effect. Microscopic examination of samples were conducted at ×200 magnification. Scale bar, 100 μm. Representative pictures and image quantification are shown. (E) Histopathological analysis of the indicated murine organs were evaluated by hematoxylin and eosin (H&E) staining at the end of the experiment (day 20 after T cell infusion). Representative photomicrographs are shown. Scale bars, 200 μm. (F) Schematic of prostate cancer cell bone metastatic xenograft model; i.v., intravenous. PC3-PSMA$^+$ tumors cells (1×10^6) were intratibially injected in the left hind leg of NSG mice, and established bone metastatic NSG models were i.v. treated with indicated CAR-T cells. The IVIS Lumina II In Vivo Imaging System was used to monitor tumor growth. (G and H) NSG mice bearing intratibial (left hind leg) PC3-PSMA$^+$ tumors were i.v. treated with 5×10^6 Ctrl T cells, Pbbz CAR-T cells, and Pbbz-LV CAR-T cells separately, and tumor growth kinetics were monitored by IVIS. Representative tumor bioluminescence images of mice on indicated days are shown (G). Overall survival of mice in each group is monitored (H). *$p < 0.05$, **$p < 0.01$, ***$p < 0.001$.

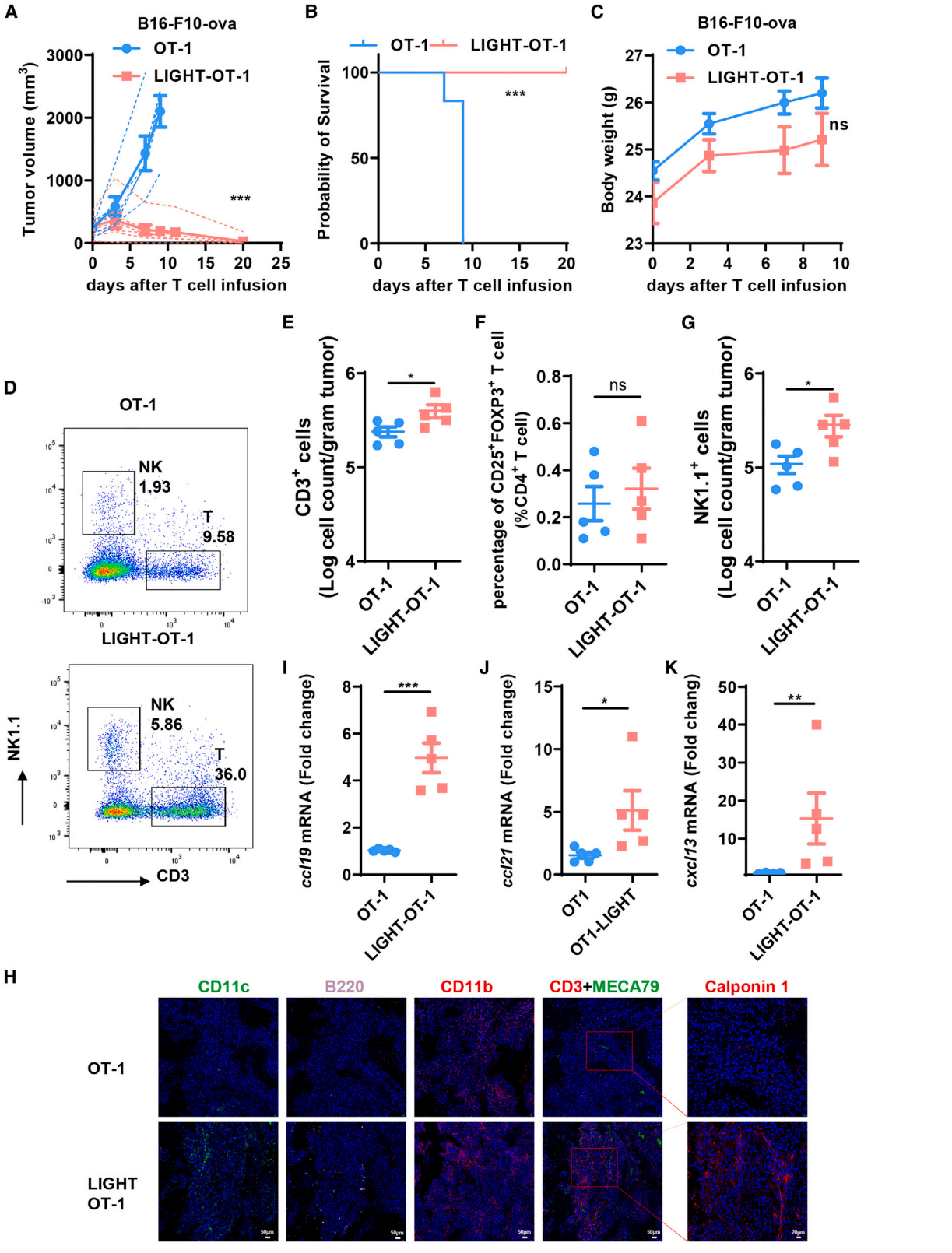

(legend on next page)

engraftment, OT-1 or LIGHT-OT-1 cells (1×10^7 cells/mouse, approximately 25% thy1.1 positive) were infused intravenously. Tumor size was monitored every 2–3 days after T cell infusion with a caliper, and body weight was measured twice a week. Tumor volume was calculated as length × width × width × 0.5, and mice were sacrificed if the tumor volume exceeded 2,000 mm^3.

Immunofluorescence staining

For investigating VTP binding to tumor blood vessels, 1×10^6 C42 cells were injected subcutaneously in the right flank of NSG mice. After 20 days, fresh established tumor tissues were submerged in 10% sucrose for 2 h, incubated in 30% sucrose overnight, and frozen in optimal cutting temperature (OCT) compound. Frozen 7-μm-thick sections were stained with FAM-labeled RGR peptides (GenScript) after masking unspecific binding sites with PBS+2% BSA for 120 min at room temperature. In some mice, sections were also stained with the vascular marker CD31 (arigo).

In some experiments, major organs were resected from the mice, fixed with neutrally buffered 4% formaldehyde, and applied to hematoxylin and eosin (H&E) staining. In some experiments, tumor tissues from treated mice at indicated endpoints were stained with anti-CD3 (Servicebio), anti-CCL21 (Bioss), anti-MECA79 (NOVUS), anti-CD11c (Servicebio), anti-CD11b (Servicebio), anti-B220 (Thermo Scientific), or anti-Calponin1 (Servicebio) antibody after formalin fixation and being embedded with paraffin (Servicebio).

Human serial sections from bone metastasized human prostate cancer tissues used in this study were kindly provided by Shanghai Changzheng Hospital. Immunohistochemical staining was done with anti-CD13, anti-PDGFRβ, anti-CD31, and anti-Pan-CK antibody. Fluorescence images were acquired with microscope and image analysis software (CaseViewer) and quantified by Image-Pro Plus 6.0.

Bioinformatic analyses and RNA-seq

Data of pan-cancer were downloaded from TCGA database (https://xenabrowser.net). Kaplan-Meier analysis based on the CXCL13 TLS gene signature in the pan-cancer cohort was performed to generate survival curve. The significance of the survival curves was done using the log rank test. The survival analysis did not show a significant difference in the overall survival rate in prostate cancer (PRAD) but did in the 5 year survival rate. The ssGSEA method of R software Gene Set Variation Analysis (GSVA) package was used to analyze the infiltration level (immune score), ESTIMATE score, tumor purity, and stromal content (stromal score) of different immune cells in prostate cancer expression profile data, and unsupervised hierarchical clustering of PRAD yields three subtypes based on the enrichment levels of the 29 immune signatures. The expression of the nine-gene TLS signature (CCL19, CCL21, CXCL13, CCR7, CXCR4, CXCR5, SELL, and LAMP3) and TNFSF14/LIGHT in trichotomized subtypes was shown by heatmap.

Total RNA of Pbbz CAR-T and Pbbz-LV CAR-T cells was collected and sequenced by BioMarker on day 14 after transduction without exposure to tumor cells. Preliminary analysis was performed using BMKCloud (www.biocloud.net), and further GSEA (leading edge analysis: Pi), differential expression analysis (edgeR), and heatmaps (gheatmap) were done by R.

Statistical analysis

All experiments were performed in triplicate and repeated at least three times, and representative results were shown. All data were mean ± SEM. p values were calculated by two-sided Student's t test or Wilcoxon test between two samples, and multiple-comparison analyses were evaluated by ANOVA (one or two way). p values <0.05 were deemed as significant.

DATA AVAILABILITY

The RNA-seq datasets generated and analyzed during the current study are not publicly available and will be available from the corresponding authors upon request.

SUPPLEMENTAL INFORMATION

Supplemental information can be found online at https://doi.org/10.1016/j.ymthe.2023.06.015.

ACKNOWLEDGMENTS

This work was supported by the National Key R&D Program of China (2018YFA0507001 to B.D.), the National Natural Science Foundation of China (32270960 to B.D., 81901608 to N.Z., 82173099 to J.Q., and 81830083 to M.L.), and the Science and Technology Commission of Shanghai Municipality (23XD1430600, 23141901800, and 23141903300). We thank East China Normal University Multifunctional Platform for Innovation (011) and Flow Cytometry Core Facility of the School of Life Sciences.

AUTHOR CONTRIBUTIONS

B.D., M.L., and N.Z. designed the project, oversaw the experiments, analyzed the data, and wrote the manuscript. X.L., J.Q., Y.S., H.X.,

Figure 7. LIGHT expression enhances the systemic anti-tumor activity in syngeneic models of solid tumors

(A and B) Syngeneic B16F10-OVA melanoma model mice were treated by i.v. injection with OT-1 or LIGHT-OT-1 cells (1×10^7 per mouse), and mean ± SEM of tumor volume (A) and survival of the mice (B) are shown after T cell infusion from two independent experiments. LIGHT-OT-1, OT-1 cells engineered to express soluble hmLIGHTt66-VTP. OT1 group: n = 6, LIGHT-OT-1 group: n = 7. Mice were euthanized when the tumor size exceeded 2,000 mm^3. (C) Body weight of mice in each group in (A). (D) Representative fluorescence-activated cell sorting (FACS) plots showing percentages of NK1.1 and CD3 in $CD45^+$ cells in the tumors of mice. (E) CD3 T cell absolute infiltration in the tumors collected from treated mice on day 7. (F) Proportions of $CD25^+FOXP3^+$ Treg cell populations in tumor tissue on day 7. (G) NK cell absolute infiltration in the tumors collected from treated mice on day 7. (H) Serial sections of tumor tissues treated with OT-1 or LIGHT-OT-1 cells were assessed by IHC with different antibodies for CD11c, B220, CD11b, CD3, MECA79, and calponin 1 signals (day 7). (I–K) Mouse *ccl19* (I), *ccl21* (J), or *cxcl13* (K) mRNA fold increases in tumor tissues from OT-1-treated B16F10-OVA melanoma tumor mice. Data are shown as the mean ± SEM. *p < 0.05, **p < 0.01, ***p < 0.001.

B.L., K.L., and C.Z. performed and analyzed the *in vitro* and *in vivo* experiments and data. C.H. performed bioinformatic analyses. J.Q. and B.T. helped to oversee the project and contributed to data analysis and editing of the final version of the manuscript. S.R. provided material support and helped to oversee the project. All authors approved the final version of the manuscript.

DECLARATION OF INTERESTS

The authors declare no competing interests.

REFERENCES

1. Park, J.H., Bienenfeld, A., Orlow, S.J., Nagler, A.R., Senechal, B., Curran, K.J., Sauter, C., Wang, Y., Santomasso, B., Mead, E., et al. (2018). Long-Term Follow-up of CD19 CAR Therapy in Acute Lymphoblastic Leukemia. N. Engl. J. Med. *19*, 449–455.
2. Mardiana, S., Solomon, B.J., Darcy, P.K., and Beavis, P.A. (2019). Supercharging adoptive T cell therapy to overcome solid tumor–induced immunosuppression. Sci. Transl. Med. *11*, eaaw2293.
3. Müller, N., Michen, S., Tietze, S., Töpfer, K., Schulte, A., Lamszus, K., Schmitz, M., Schackert, G., Pastan, I., and Temme, A. (2015). Engineering NK Cells Modified With an EGFRvIII-specific Chimeric Antigen Receptor to Overexpress CXCR4 Improves Immunotherapy of CXCL12/SDF-1alpha-secreting Glioblastoma. J. Immunother. *38*, 197–210.
4. Almåsbak, H., Rian, E., Hoel, H.J., Pulè, M., Wälchli, S., Kvalheim, G., Gaudernack, G., and Rasmussen, A.-M. (2011). Transiently redirected T cells for adoptive transfer. Cytotherapy *13*, 629–640.
5. Comerford, I., Harata-Lee, Y., Bunting, M.D., Gregor, C., Kara, E.E., and McColl, S.R. (2013). A myriad of functions and complex regulation of the CCR7/CCL19/CCL21 chemokine axis in the adaptive immune system. Cytokine Growth Factor Rev. *24*, 269–283.
6. Adachi, K., Kano, Y., Nagai, T., Okuyama, N., Sakoda, Y., and Tamada, K. (2018). IL-7 and CCL19 expression in CAR-T cells improves immune cell infiltration and CAR-T cell survival in the tumor. Nat. Biotechnol. *36*, 346–351.
7. Luo, H., Su, J., Sun, R., Sun, Y., Wang, Y., Dong, Y., Shi, B., Jiang, H., and Li, Z. (2020). Coexpression of IL7 and CCL21 Increases Efficacy of CAR-T Cells in Solid Tumors without Requiring Preconditioned Lymphodepletion. Clin. Cancer Res. *26*, 5494–5505.
8. Martinez-Usatorre, A., and De Palma, M. (2020). A LIGHTning Strike to the Metastatic Niche. Cell Rep. *30*, 599–601.
9. Skeate, J.G., Otsmaa, M.E., Prins, R., Fernandez, D.J., Da Silva, D.M., and Kast, W.M. (2020). TNFSF14: LIGHTing the Way for Effective Cancer Immunotherapy. Front. Immunol. *11*, 922.
10. Granger, S.W., and Rickert, S. (2003). LIGHT–HVEM signaling and the regulation of T cell-mediated immunity. Cytokine Growth Factor Rev. *14*, 289–296.
11. Soroosh, P., Doherty, T.A., So, T., Mehta, A.K., Khorram, N., Norris, P.S., Scheu, S., Pfeffer, K., Ware, C., and Croft, M. (2011). Herpesvirus entry mediator (TNFRSF14) regulates the persistence of T helper memory cell populations. J. Exp. Med. *208*, 797–809.
12. Wang, J., Lo, J.C., Foster, A., Yu, P., Chen, H.M., Wang, Y., Tamada, K., Chen, L., and Fu, Y.-X. (2001). The regulation of T cell homeostasis and autoimmunity by T cell–derived LIGHT. J. Clin. Invest. *108*, 1771–1780.
13. Lee, Y., Chin, R.K., Christiansen, P., Sun, Y., Tumanov, A.V., Wang, J., Chervonsky, A.V., and Fu, Y.X. (2006). Recruitment and activation of naive T cells in the islets by lymphotoxin beta receptor-dependent tertiary lymphoid structure. Immunity *25*, 499–509.
14. Schneider, K., Potter, K.G., and Ware, C.F. (2004). Lymphotoxin and LIGHT signaling pathways and target genes. Immunol. Rev. *202*, 49–66.
15. Girard, J.P., Moussion, C., and Förster, R. (2012). HEVs, lymphatics and homeostatic immune cell trafficking in lymph nodes. Nat. Rev. Immunol. *12*, 762–773.
16. Petitprez, F., de Reyniès, A., Keung, E.Z., Chen, T.W.W., Sun, C.M., Calderaro, J., Jeng, Y.M., Hsiao, L.P., Lacroix, L., Bougoüin, A., et al. (2020). B cells are associated with survival and immunotherapy response in sarcoma. Nature *577*, 556–560.
17. He, Y., Jiang, Z., Chen, C., and Wang, X. (2018). Classification of triple-negative breast cancers based on Immunogenomic profiling. J. Exp. Clin. Cancer Res. *37*, 327.
18. Kloss, C.C., Lee, J., Zhang, A., Chen, F., Melenhorst, J.J., Lacey, S.F., Maus, M.V., Fraietta, J.A., Zhao, Y., and June, C.H. (2018). Dominant-Negative TGF-beta Receptor Enhances PSMA-Targeted Human CAR T Cell Proliferation And Augments Prostate Cancer Eradication. Mol. Ther. *26*, 1855–1866.
19. Granger, S.W., Butrovich, K.D., Houshmand, P., Edwards, W.R., and Ware, C.F. (2001). Genomic characterization of LIGHT reveals linkage to an immune response locus on chromosome 19p13.3 and distinct isoforms generated by alternate splicing or proteolysis. J. Immunol. *167*, 5122–5128.
20. Tang, H., Wang, Y., Chlewicki, L.K., Zhang, Y., Guo, J., Liang, W., Wang, J., Wang, X., and Fu, Y.X. (2016). Facilitating T Cell Infiltration in Tumor Microenvironment Overcomes Resistance to PD-L1 Blockade. Cancer Cell *30*, 285–296.
21. Joyce, J.A., Laakkonen, P., Bernasconi, M., Bergers, G., Ruoslahti, E., and Hanahan, D. (2003). Stage-specific vascular markers revealed by phage display in a mouse model of pancreatic islet tumorigenesis. Cancer Cell *4*, 393–403.
22. He, B., Jabouille, A., Steri, V., Johansson-Percival, A., Michael, I.P., Kotamraju, V.R., Junckerstorff, R., Nowak, A.K., Hamzah, J., Lee, G., et al. (2018). Vascular targeting of LIGHT normalizes blood vessels in primary brain cancer and induces intratumoural high endothelial venules. J. Pathol. *245*, 209–221.
23. He, B., Johansson-Percival, A., Backhouse, J., Li, J., Lee, G.Y.F., Hamzah, J., and Ganss, R. (2020). Remodeling of Metastatic Vasculature Reduces Lung Colonization and Sensitizes Overt Metastases to Immunotherapy. Cell Rep. *30*, 714–724.e5.
24. Zhai, Y., Guo, R., Hsu, T.L., Yu, G.L., Ni, J., Kwon, B.S., Jiang, G.W., Lu, J., Tan, J., Ugustus, M., et al. (1998). LIGHT, a novel ligand for lymphotoxin beta receptor and TR2/HVEM induces apoptosis and suppresses in vivo tumor formation via gene transfer. J. Clin. Invest. *102*, 1142–1151.
25. Harrop, J.A., Reddy, M., Dede, K., Brigham-Burke, M., Lyn, S., Tan, K.B., Silverman, C., Eichman, C., DiPrinzio, R., Spampanato, J., et al. (1998). Antibodies to TR2 (Herpesvirus Entry Mediator), a New Member of the TNF Receptor Superfamily, Block T Cell Proliferation, Expression of Activation Markers, and Production of Cytokines. J. Immunol. *161*, 1786–1794.
26. Dejardin, E., Droin NM., Delhase M, Haas, E., Cao, Y., Makris, C., Li, Z.-W., Karin, M., Ware, C.F., Green, D.R. The lymphotoxin-beta receptor induces different patterns of gene expression via two NF-kappaB pathways.Immunity 17 525-535
27. Yoshida, R., Nagira, M., Imai, T., Baba, M., Takagi, S., Tabira, Y., Akagi, J., Nomiyama, H., and Yoshie, O. (1998). EBI1-ligand chemokine (ELC) attracts a broad spectrum of lymphocytes: activated T cells strongly up-regulate CCR7 and efficiently migrate toward ELC. Int. Immunol. *10*, 901–910.
28. Förster, R., Davalos-Misslitz, A.C., and Rot, A. (2008). CCR7 and its ligands: balancing immunity and tolerance. Nat. Rev. Immunol. *8*, 362–371.
29. Denton, A.E., Innocentin, S., Carr, E.J., Bradford, B.M., Lafouresse, F., Mabbott, N.A., Mörbe, U., Ludewig, B., Groom, J.R., Good-Jacobson, K.L., and Linterman, M.A. (2019). Type I interferon induces CXCL13 to support ectopic germinal center formation. J. Exp. Med. *216*, 621–637.
30. Chang, Y.H., Hsieh, S.L., Chao, Y., Chou, Y.C., and Lin, W.W. (2005). Proinflammatory effects of LIGHT through HVEM and LTbetaR interactions in cultured human umbilical vein endothelial cells. J. Biomed. Sci. *12*, 363–375.
31. Larson, R.C., Kann, M.C., Bailey, S.R., Haradhvala, N.J., Llopis, P.M., Bouffard, A.A., Scarfó, I., Leick, M.B., Grauwet, K., Berger, T.R., et al. (2022). CAR T cell killing requires the IFNgammaR pathway in solid but not liquid tumours. Nature *604*, 563–570.